Journal of Cellular Physiology

Kinetic Properties of ASC Protein Aggregation in Epithelial Cells

JUN CHENG,[1] ANDREA L. WAITE,[2] ERIC R. TKACZYK,[3] KEVIN KE,[1] NEIL RICHARDS,[2] ALAN J. HUNT,[1,3]* AND DEBORAH L. GUMUCIO[2]**

[1]*Department of Biomedical Engineering, University of Michigan, Ann Arbor, Michigan*

[2]*Department of Cell and Developmental Biology, University of Michigan, Ann Arbor, Michigan*

[3]*Center for Ultrafast Optical Science, University of Michigan, Ann Arbor, Michigan*

Apoptosis-associated speck-like protein with CARD domain (ASC), an adaptor protein composed of caspase recruitment and pyrin domains, can efficiently self-associate to form a large spherical structure, called a speck. Although ASC aggregation is generally involved with both inflammatory processes and apoptosis, the detailed dynamics of speck formation have not been characterized. In this report, speck formation in HeLa cells transfected with ASC is examined by time-lapse live-imaging by confocal laser scanning microscopy. The results show that ASC aggregation is a very rapid and tightly regulated process. Prior to speck formation, soluble ASC aggregation is a low probability event, and the affinity of ASC subunits for one another is very low. Following a speck nucleation event, the affinity for further addition of ASC subunits increases dramatically, and aggregation is a highly energetically favorable reaction (Gibbs free energy ~ -40 kJ/mol). This leads to a rapid depletion of soluble ASC, making it highly unlikely that a second speck will form inside the same cell and assuring that speck formation is "all or none," with a well-defined end point. Comparison with kinetic models of the aggregation process indicates diffusion, instead of active transport, is the dominant process for speck growth. Though speck formation and aggresome formation share some properties, we show that the two processes are distinct.

J. Cell. Physiol. 222: 738–747, 2010.

Many cellular activities, from actin filament assembly to cell-cycle progression, depend on regulated aggregation of proteins. A particularly striking example of controlled protein complex assembly is provided by the inflammasome (Petrilli et al., 2007). For this multiprotein complex, triggered protein aggregation is akin to throwing a molecular switch that activates caspase-1 and promotes robust IL-1β processing. In myeloid cells, activation of the inflammasome can lead within minutes to an inflammatory death process called pyroptosis (Fernandes-Alnemri et al., 2007). The dramatic outcome of this regulated aggregation event demands a thorough understanding of the means by which such complexes form.

Several different types of inflammasome complex have been identified, all of which are built on the same central platform: the ASC or PyCard protein. ASC is a simple adaptor protein that consists of two linked protein–protein interaction domains of the death domain superfamily: a PyD or pyrin domain and a CARD or caspase recruitment domain. These two domains of ASC are used to link sensor and effector molecules to effectively and rapidly assemble the inflammasome. For example, in the case of the Nalp3 inflammasome, the Nalp3 protein senses a variety of activators (specific bacterial wall proteins, certain microbial toxins, ATP, and monosodium urate) and responds by self-oligomerizing (Martinon, 2008). Nalp3 contains an N-terminal PyD that interacts with the PyD of ASC; thus oligomerization of Nalp3 promotes ASC agglutination. Through its CARD, ASC can recruit and activate caspase-1, resulting in the potent production and processing of IL-1β. The Nalp3/ASC/caspase-1 inflammasome is particularly interesting as its malfunction appears to underlie several human diseases, including three autoinflammatory syndromes caused by mutations in Nalp3 (Muckle Wells Syndrome, Familial Cold Urticaria, and Neonatal Multisystem Inflammatory Disease) (Mariathasan et al., 2006) as well as two arthritic conditions thought to represent problems with Nalp3 inflammasome sensing or effector function (gout and pseudogout) (Martinon et al., 2006).

The ASC adaptor facilitates the formation of large perinuclear agglutinations that have been called "specks" (Masumoto et al., 1999). Recent data indicate that specks represent active inflammasomes (Fernandes-Alnemri et al., 2007). Mature specks are spherical perinuclear structures, 1–3 μm in diameter that appear to be composed of tightly wound filaments (Masumoto et al., 1999; Richards et al., 2001). In myeloid cells lacking specks, but expressing ASC, the cellular content of ASC is diffusely located throughout the nucleus and cytoplasm (Richards et al., 2001; Fernandes-Alnemri et al., 2007). Once inflammasome activity is stimulated, nearly all of this distributed ASC is collected into a single perinuclear speck structure in less than 3 min (Fernandes-Alnemri et al., 2007).

Specks that form in myeloid cells, which contain caspase-1, rapidly transition from inflammasomes into pyroptosomes (Fernandes-Alnemri et al., 2007). This inflammatory death

Jun Cheng and Andrea L. Waite contributed equally to this work.

Additional Supporting Information may be found in the online version of this article.

Contract grant sponsor: National Institute of Health;
Contract grant numbers: R01-GM072006, R01-AI53262.

*Correspondence to: Alan J. Hunt, Associate Professor, Department of Biomedical Engineering, University of Michigan College of Engineering, 1101 Beal Avenue, Box 2170, Ann Arbor, MI 48109-2099. E-mail: ajhunt@umich.edu

**Correspondence to: Deborah L. Gumucio, Professor, Department of Cell and Developmental Biology, University of Michigan Medical School, 109 Zina Pitcher Place, Box 2200, Ann Arbor, MI 48109-2200. E-mail: dgumucio@umich.edu

Received 20 August 2009; Accepted 2 November 2009

Published online in Wiley InterScience (www.interscience.wiley.com.), 17 December 2009.
DOI: 10.1002/jcp.22005

process, previously described in macrophages infected with intracellular viral or bacterial pathogens, is characterized by plasma membrane swelling and rupture followed by nuclear condensation and loss of mitochondrial potential (Swanson and Molofsky, 2005; Fink and Cookson, 2006). Thus, the formation of the ASC speck/pyroptosome structure is the apparent activating event for a cascade of three events: caspase-1 activation, IL-1β processing, and pyroptosis. None of these processes occur in cells without specks (Fernandes-Alnemri et al., 2007; Fernandes-Alnemri and Alnemri, 2008). Importantly, the ASC speck itself is not "garbage" secondary to caspase activation, as specks continue to form in the presence of potent inhibitors of caspase activity (McConnell and Vertino, 2000; Gumucio et al., 2002).

Though ASC speck formation, inflammasome activity, and pyroptosis in response to intracellular pathogens are all critical processes in myeloid cells, ASC is also expressed in many epithelial tissues where it has been postulated to play a role in cell differentiation. Interestingly, in a variety of epithelial cancers including tumors in the breast (Conway et al., 2000; Moriai et al., 2002; Virmani et al., 2003), skin (Guan et al., 2003), colon (Yokoyama et al., 2003), stomach (Moriai et al., 2002), ovary (Akahira et al., 2004; Terasawa et al., 2004), prostate (Alumkal et al., 2008), and lung (Virmani et al., 2003) ASC gene expression is frequently quelled by methylation-induced silencing, suggesting a tumor suppressor role in these tissues. Specks have not been demonstrated in epithelial tissues in vivo, most likely because of the low probability of observing the 2 μm speck structure in a histological section. However, transfection of ASC causes speck formation in many cell types, including HeLa, 293, and COS cells (Masumoto et al., 1999; Richards et al., 2001); thus the ability of ASC to form specks appears to be an innate property of this protein, and one that, as demonstrated in myeloid cells, is integral to its function.

In epithelial cells as well as myeloid cells, the formation of ASC specks is associated with cell death (Masumoto et al., 1999; Schaner et al., 2001; Fernandes-Alnemri et al., 2007; Balci-Peynircioglu et al., 2008). However, death follows many hours or even days after speck formation in HeLa or COS cells (Schaner et al., 2001), in contrast to minutes after speck formation in myeloid cells (Fernandes-Alnemri et al., 2007). In addition, since caspase-1 is expressed at low concentrations or not at all in many non-myeloid cells, the mechanism of cell death following speck formation must differ from the caspase-1-mediated process seen in myeloid cells.

To begin to investigate the process of speck formation in epithelial cells, we examined the dynamics of speck formation in HeLa cells transfected with ASC-YFP. In addition, since specks highly resemble perinuclear structures called aggresomes (Opazo et al., 2008), we examined ASC specks for the expression of several markers of aggresome formation. Aggresomes are large perinuclear collections of misfolded proteins that dynamically form and are subsequently dismantled by lysosomes during autophagy (Opazo et al., 2008).

The data reported here indicate that speck formation in HeLa cells is a process distinct from aggresome formation. In addition, we report for the first time that specks can form in both the cytosolic and nuclear compartments. Kinetic models of the process allow us to reject active transport as a primary process for speck growth, and posit that rapid speck formation is limited by the rate that ASC subunits diffuse to the speck surface. The nucleation event that initiates ASC speck formation in epithelial cells is likely to be a tightly regulated process.

Materials and Methods

Cell culture and transfection

HeLa cells were cultured in Dulbecco's modified Eagle medium (Gibco by Invitrogen, Carlsbad, CA) supplemented with 10% (v/v) fetal bovine serum. For experiments, cells were plated either on sterile glass coverslips in six-well plates (for immunofluorescence) or in glass-bottom 35 mm culture plates for live cell imaging (MatTek, Ashland, MA). Cells were transfected using FUGENE-6 (Roche Applied Science, Indianapolis, IN) and incubated for 16–20 h before analysis.

Plasmids and antibodies

ASC-YFP was generated using the pE-YFP-1 vector from Clontech (Mountain View, CA). The rabbit polyclonal anti-proteasome 20S C2 antibody was obtained from Abcam (Cambridge, MA), and the mouse monoclonal anti-vimentin antibody was obtained from Sigma (St. Louis, MO). Goat α-mouse AF568 and goat α-rabbit AF568 were purchased from Molecular Probes (by Invitrogen, Eugene, OR).

Immunofluorescence

Cultures were fixed using 4% paraformaldehyde in PBS for 30 min. Cells were then permeabilized using 0.2% Triton X-100 in PBS, and blocked with a solution containing 10% goat serum, 1% bovine serum albumin, and 0.1% Tween-20 in PBS. Primary and secondary antibody application was carried out, and nuclei were counterstained with DAPI. Coverslips were mounted on slides using a ProLong Antifade Kit (Molecular Probes by Invitrogen) and allowed to dry in the dark for several hours. Slides were visualized using a Leica TCS SP5 confocal microscope with an oil immersion objective (63×, NA = 1.4), and images were processed using Adobe Photoshop.

Confocal scanning laser microscopy

Sixteen to 20 h after transfection, the HeLa cells were changed to L-15 medium supplemented with 10% fetal bovine serum and were placed on a confocal scanning laser microscope (Leica TCS SP2) for imaging. The specimen stage and culture plate were kept at 37°C, and the confocal room was kept dark during laser scanning. Images were taken using an oil-immersion objective (HCX PL APO CS, 40×, NA = 1.25). As shown by comparing the fluorescence decay of a non-speck-forming HeLa cell with that of a speck-forming cell in the same field, photobleaching was minimal.

Imaging analysis

An automatic program was used to analyze the time-lapse image sequences. The program was written based on image processing algorithm in Vision (National Instruments Co., Austin, TX). The final speck size was measured after all ASC aggregated to form a speck, that is, the fluorescence intensity inside cells dropped below the detection limit compared with background. For an image sequence, the location of interest was measured by the distance from the speck center. In the figures, the distance is scaled to the final speck radius in order to simplify the comparison with simulation results. After the location was selected for one image, fluorescence intensity over an area (no smaller than 3 × 3 pixels, and no bigger than 10 × 10 pixels) was averaged to suppress noise. The averaged fluorescence intensity per pixel was calculated image by image automatically by the program. This procedure was repeated at all locations of interest. Finally, the fluorescence intensities at various locations were plotted as a function of time.

Total cytosolic protein measurement

At 80% confluence, HeLa cells were harvested and washed in PBS twice. The cells were suspended in ice-cold hypotonic buffer A (10 mM HEPES, pH 8.0, 1.5 mM $MgCl_2$, 10 mM KCl, and 1 mM DTT) and were swollen on ice for 15 min. After the cell membranes were disrupted by five strokes through 25-gauge syringe, the homogenate was centrifuged (10,000 rpm, 20 sec) and the supernatant (cytosolic fraction) was harvested. The protein concentration of this supernatant was measured using standard Bradford protein assay.

Results

Two different distributions of ASC in transfected HeLa cells

HeLa cells were transfected with ASC-YFP and a field of cells was imaged by confocal microscopy 18–20 h later. At this time, 47% of transfected cells contained a single "speck" of aggregated ASC. In speck-containing cells, the cytosolic ASC-YFP signal was close to background and an intense fluorescent signal was present in the perinuclear speck, as shown in Figure 1A (cells outlined with dotted lines). In contrast, in transfected cells lacking specks, ASC fluorescence was uniformly distributed throughout the cell (both cytoplasm and nucleus, Fig. 1B). In such cells, the concentration ratio for ASC in the nucleus compared to that in the cytoplasm was 1.02 ± 0.12 (mean $\pm$ SD), as determined by average fluorescence intensity from 35 HeLa cells (shown in Fig. 1C). No "hot spots" of concentrated ASC signal were detectable in cells without specks.

Comparison of ASC specks with aggresomes

Given the similarity in size and location between aggresomes and ASC specks (comparing Figure 3 in Opazo et al., 2008, to Figure 2 in Richards et al., 2001), we examined the possibility that the speck may actually represent an aggresome. HeLa cells were transfected with ASC-YFP, and 24 h later, cells were fixed and stained with antibodies against two proteins known to be associated with aggresomes: the 20S subunit of the proteasome (Garcia-Mata et al., 1999) and vimentin, an intermediate filament protein (Johnston et al., 1998). We found that similar to aggresomes, specks are found in cells containing an assembled proteasome, and that the speck co-localizes with the forming proteasome (Fig. 2A,B). Another characteristic feature of the aggresome is that upon its formation, the vimentin filament network completely collapses around it (Johnston et al., 1998; Garcia-Mata et al., 1999). However, speck formation does not cause the vimentin network to collapse, though there is some apparent co-localization of vimentin at the surface of the speck (Fig. 2C,D). Thus, specks share some but not all characteristics of aggresomes. To further probe this question, we next compared the kinetics of speck formation in non-myeloid cells with published information on the formation of aggresomes (Opazo et al., 2008).

ASC rapidly aggregates to form a speck

Using time-lapse video recording, we investigated the ASC aggregation process in epithelial (HeLa) cells by following the redistribution of ASC-YFP fluorescence intensity during speck

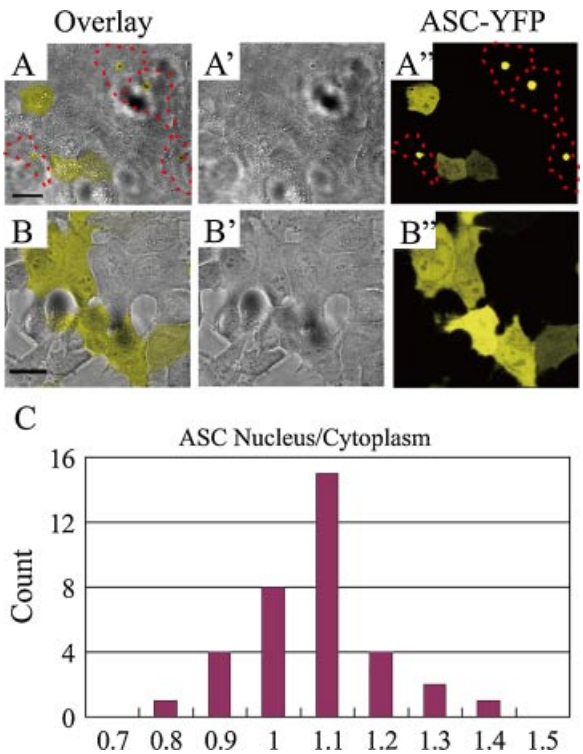

Fig. 1. ASC distribution throughout cytoplasm and nucleus. A,B: Confocal images of ASC-YFP transfected HeLa cells, where A and B are overlays of bright field image (A′,B′) and ASC-YFP fluorescence images (A″,B″). Cells in which specks have formed are outlined by a red dashed line. Scale bar: 20 μm. C: Histogram of the ratio of ASC-YFP fluorescence intensity in the cytoplasm to that inside nucleus prior to speck formation. A total of 35 transfected HeLa cells were analyzed. [Color figure can be viewed in the online issue, which is available at www.interscience.wiley.com.]

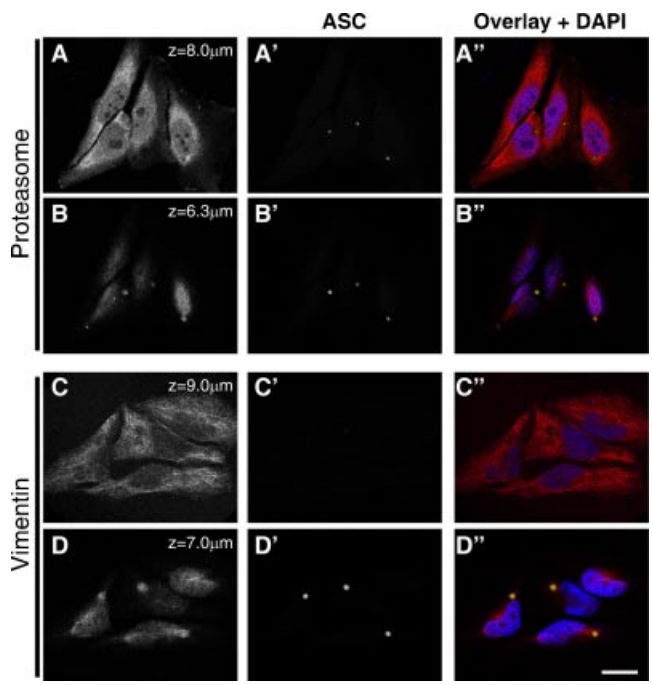

Fig. 2. Specks share some but not all characteristics of aggresomes. A,B: HeLa cells were transfected with ASC-YFP and incubated for 24 h to allow speck formation (green). The proteasome was visualized using an antibody to the alpha subunit (red). Only cells that have assembled proteasomes exhibit specks and specks co-localize with the forming proteasome. Parts A, A′, and A″ show proteasome staining, ASC staining, and merged images, respectively, for a confocal slice near the bottom of the cell. Parts B, B′, and B″ represent the same cell, but images are obtained from a slice near the top of the cell, where the proteasome is forming. C,D: Transfected HeLa cells were stained with anti-vimentin (red) to visualize intermediate filaments. Though intermediate filaments are known to collapse around aggresomes, speck formation does not seem to alter the distribution of intermediate filaments. Parts C, C′, and C″ represent staining for vimentin, ASC, and merged images, respectively, from a confocal slice near the bottom of the cell, showing an intact vimentin network. Parts D, D′, and D″ represent the same staining in a region near the top of the cell where the speck resides. Though some co-localization of vimentin and ASC is visible, the vimentin network is not collapsed around the speck. Scale bar: 20 μm. [Color figure can be viewed in the online issue, which is available at www.interscience.wiley.com.]

formation (see Movie S1 and S2). As shown in Figure 3A, specks grow rapidly after nucleation, and within 100 sec, the ASC fluorescence intensity throughout the cytoplasm is largely depleted, confirming earlier reports of the rapidity of speck formation in THP-1 macrophages (Fernandes-Alnemri et al., 2007). The fluorescence intensity inside the cytoplasm decays with a time constant (τ) of 46.4 ± 0.8 sec. By contrast, the ASC fluorescence intensity inside the nucleus decreases at nearly an order of magnitude slower rate, $\tau = 409 \pm 10$ sec and requires over 700 sec to decrease to background levels. A three-dimensional structural reconstruction of mature specks by confocal z-scan indicates a solid spherical structure (data not shown), suggesting that specks grow by accumulation of ASC across their surface.

HeLa cells can be multinucleate. When speck aggregation occurs in binucleate cells, the ASC fluorescence inside both nuclei distributes uniformly and depletes at the same rate (Fig. 3B). This suggests that nuclear depletion rate is determined by a stable reproducible factor such as the rate of transport through nuclear pores.

In cases where a speck forms very near the nucleus, such that the location is not easy to determine visually, a much faster ASC-YFP depletion from the cytoplasm versus the nucleus provides evidence for a cytoplasmic location; as shown in

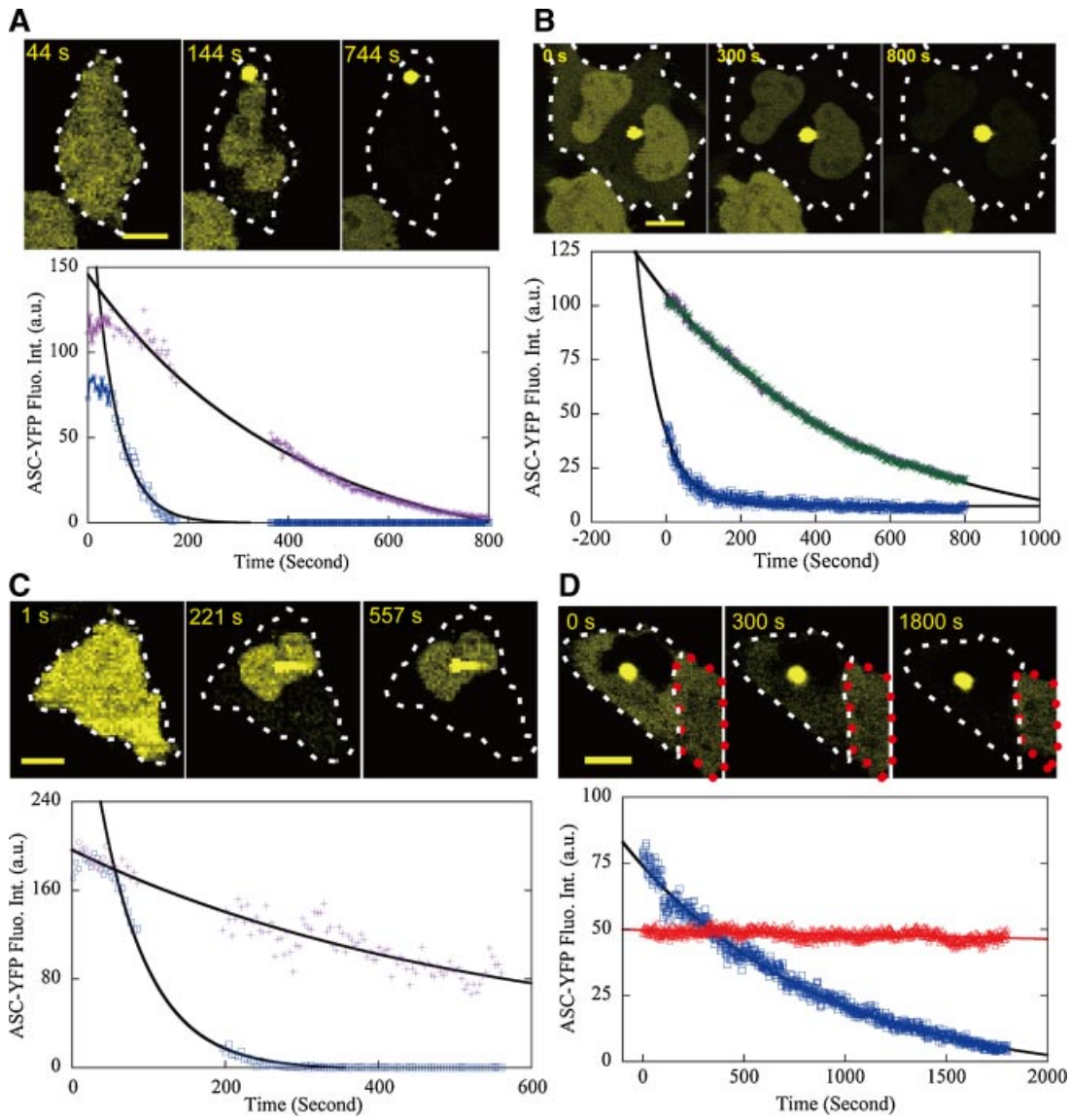

Fig. 3. Examples of the speck formation process. "□" blue data points for cytoplasm and "+" purple (and "×" green) for nucleus. The solid curves are single exponential fits. All scale bars are 10 μm. A: Typical perinuclear speck formation. The ASC fluorescence depletion time constant was $\tau = 46.4 \pm 0.8$ sec for the cytoplasm and $\tau = 409 \pm 10$ sec for the nucleus. B: Speck formation inside a HeLa cell with two nuclei, where "+" ("×") indicates the upper-left (lower-right) nucleus, respectively. The ASC fluorescence intensity in the nucleus and cytoplasm was independently monitored and plotted: $\tau = 64 \pm 2$ sec for the cytoplasm and $\tau = 529 \pm 6$ sec for the nucleus. C: Speck formation overlapping the nucleus. The cytoplasmic location of the speck was indicated by the different time constants in cytoplasm ($\tau = 64 \pm 2$ sec) and the nucleus ($\tau = 851 \pm 487$ sec). D: Speck formation inside the nucleus. ASC fluorescence intensity depleted initially inside the nucleus and was followed by a much slower depletion in the cytoplasm ($\tau = 950 \pm 16$ sec). The red dotted line indicates a non-speck-forming cell serving as a control next to the speck-forming cell, and "Δ" red data points are the ASC fluorescence intensity for the control cell. [Color figure can be viewed in the online issue, which is available at www.interscience.wiley.com.]

Figure 3C, ASC depletion from the cytoplasm is ~10 times faster than from the nucleus.

Occasionally, speck formation occurs inside the nucleus, as shown in Figure 3D. In this case, ASC is first rapidly depleted inside the nucleus; secondarily, ASC depletion in the cytoplasm proceeds at a much slower rate, $\tau = 950 \pm 16$ sec, most likely determined by the rate of transport of ASC from cytoplasm into the nucleus. Photobleaching during confocal scanning is negligible, as evidenced by the fact that ASC fluorescence intensity of an adjacent non-speck forming, ASC-positive cell in the same field of view decreased with a time constant of 12 h, equivalent to less than 0.01% photobleaching per laser scan (Fig. 3D).

ASC is depleted at the same rate throughout the cytoplasm

To determine the kinetics of ASC redistribution during speck formation, the fluorescence intensity was followed at various locations within the cytoplasm by high-resolution confocal live-cell-imaging (Fig. 4). The rate of ASC depletion shows little, if any dependence on the location within the cytoplasm, and is surprisingly independent of the distance from the speck (Fig. 4B,E). This independence is also apparent in plots of the fluorescence intensity profile along a line projected across cells, as shown in Figure 4C,F. For each cross-section profile, a flat curve of ASC-YFP fluorescence intensity is observed within the cytoplasm, the nucleus, or speck. Thus, although the level of intensity within these three compartments differs dramatically, the ASC distribution within each compartment remains homogeneous throughout the process of speck formation.

The rate of ASC depletion from the nucleus is also uniform throughout the nucleus, though substantially slower than in the cytoplasm (Fig. 5). This is apparent both from fluorescence decay curves at different locations inside the nucleus (Fig. 5B,E), and cross-section fluorescence profiles (Fig. 5C,F).

Simulation of speck formation: A two-step ASC aggregation process

It is likely that ASC dimers, rather than ASC monomers, oligomerize to form a speck (Fernandes-Alnemri et al., 2007). Therefore, in the following analysis, soluble ASC is assumed to exist as dimers. The ASC aggregation process can be expressed by a simple chemical kinetic equation:

$$\text{free ASC} + (\text{speck})_n \underset{k_{OFF}}{\overset{k_{ON}}{\rightleftharpoons}} (\text{speck})_{n+1}$$

where $(\text{speck})_n$ is the speck containing n ASC dimers, k_{ON} is the first-order on-rate constant, and k_{OFF} is the zero-order off-rate. Thus, once a speck has formed, the rate of ASC aggregation depends on the ASC concentration and reaches equilibrium when the concentration drops to equal the inverse of the equilibrium rate constant ($K_{EQ} = k_{ON}/k_{OFF}$). However, before equilibrium is established, the rate of aggregation will depend on the concentration of ASC in the local vicinity of the speck. Thus, we consider a two-step model for the process for ASC aggregation onto a speck following nucleation: (1) ASC dimers diffuse randomly until they encounter a growing speck surface. This process can be modeled as a general diffusion process, which will be discussed in detail later. (2) Soluble ASC dimers bind to the speck surface. The latter step is limited by the rate that ASC orients to the geometry of specific binding sites on the speck surface, and the energy barrier of bond formation. This process can be modeled by an effective binding efficiency K_B, which describes the probability that an ASC dimer that encounters a speck will bind.

Assuming that free ASC proteins arrive at the speck surface by diffusion, the diffusion process is governed by the differential equation $(\partial C/\partial t) = D\nabla^2 C$, where C is the concentration of free ASC protein and D is the diffusion coefficient of ASC protein. Since the molecular weight (MW) of ASC is 22 kDa (Masumoto et al., 1999; Richards et al., 2001), the diffusion coefficient is estimated to be 70 μm^2/sec for an ASC-YFP monomer (49 kDa) and 59 μm^2/sec for the ASC-YFP dimer, based on the diffusion coefficients for similar sized proteins (Tyn and Gusek, 1990), where the viscosity of cytoplasm is taken as similar to water (Fushimi and Verkman, 1991; Luby-Phelps et al., 1993).

Since HeLa cells during interphase are thinly but broadly spread on the dish, we have simplified the mathematical simulations by modeling the speck/cell structure as a flat cylinder with the speck concentric at the cell center (see Supporting Information for detailed discussion). The simulation focuses on the diffusion of ASC dimers to a speck located in the cytosol, with the contribution from ASC inside the nucleus neglected because of the much slower time constant of depletion. For initial conditions, ASC is evenly distributed throughout the cell. After the speck nucleation event occurs, free ASC moves through the cell, as governed by the diffusion equation, until it becomes immobilized by aggregating onto the speck. The speck volume grows in proportion to the total aggregated ASC protein, scaled such that the final speck diameter is similar to experimental observations. During simulations, boundary conditions are set so that no new ASC flows into the cell from outside of the cell boundary, no ASC inside the speck disassociates back into the cytoplasm (i.e., $k_{OFF} \sim 0$), and no new ASC proteins are synthesized by the cell.

To simulate the ASC diffusion and aggregation process, the time-derivative diffusion equation is solved numerically using the standard Gauss–Seidel method, as implemented in MatLab (by The MathWorks, Natick, MA). Values of the binding efficiency, K_B, and the diffusion coefficient, D, are selected so that the simulated decay time closely matches the experimentally observed time constant for depletion of soluble ASC. Since the diffusion coefficient predicted from the molecular weight of ASC-YFP dimers is ~60 μm^2/sec, or 70 μm^2/sec for monomers, only diffusion coefficients near to these values are considered. Figure 6 shows the results for extreme values of K_B, which still allowed the experimentally observed decay time to be reproduced using reasonable values for the diffusion coefficient.

Figure 6A shows simulated ASC depletion at various distances from the speck, assuming a binding efficiency $K_B = 100\%$, and diffusion coefficient D = 40 μm^2/sec. The simulated ASC concentration at several locations (2r, 4r, and 8r, where r is the mature speck radius) is plotted as a function of time, and a single exponential decay fitting to the 2r curve yields a time constant of 52 sec, consistent with our experimental observations. To a first approximation, the predicted time constant of ASC depletion varies inversely with the diffusion coefficient. The experimentally observed time constant can only be made consistent with simulation using diffusion coefficients predicted from molecular weights similar to that of ASC-YFP; this suggests a diffusion-limited process for ASC transport and aggregation.

However, when the binding efficiency is high (Fig. 6A) the simulation curves predict different time constants for ASC depletion at different locations within the cell: slower depletion occurs at locations further away from the speck. This finding is contrary to the location-independent ASC decay rate that is observed experimentally (see Fig. 4). The simulation is brought into agreement with the observational data by substantially decreasing the binding efficiency to $K_B = 10\%$. To match the

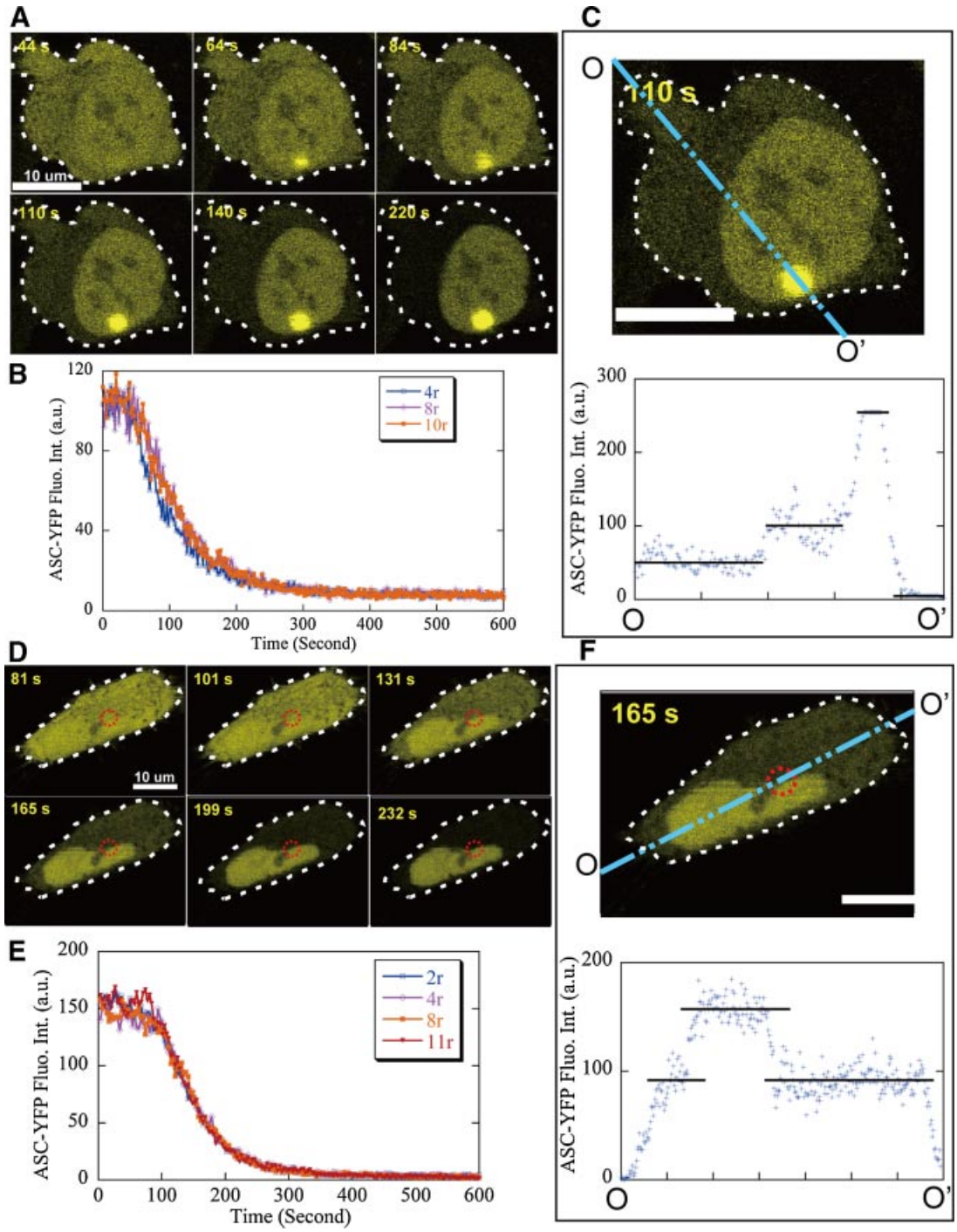

Fig. 4. ASC depletion rate is the same at all locations within the cytoplasm. The cytoplasmic locations are labeled by their distance from the speck center and scaled by the corresponding mature speck radius (r). All scale bars are 10 μm. A–C: Cytoplasmic ASC depletion with the speck visible on the same focal plane. A: Time-lapse image sequences. B: ASC fluorescence intensity at different cytoplasmic locations as a function of time ($\tau = 73.6 \pm 0.4$ sec). C: A cross-section profile of ASC fluorescence intensity. D–F: Cytoplasmic ASC depletion with the speck on a different focal plane. D: Time-lapse image sequences, where the dashed circle indicates the speck location at a different focal plane. E: ASC fluorescence intensity at different cytoplasmic locations as a function of time ($\tau = 67.6 \pm 0.4$ sec). F: A cross-section profile of ASC fluorescence intensity. [Color figure can be viewed in the online issue, which is available at www.interscience.wiley.com.]

experimentally observed decay time, the diffusion coefficient is then raised to $D = 80\ \mu m^2/sec$, which is still reasonably close to the diffusion coefficient predicted from the molecular weight (Fig. 6B). Simulation with this set of parameters yields almost homogeneous ASC concentration at different locations, and the time constant of the single exponential decay is 56 sec. Additional simulations with varying K_B show that ASC becomes more homogeneous as K_B is further reduced, but at the cost of an increasing, but unlikely, large diffusion coefficients in order to prevent the decay time from becoming inconsistent with

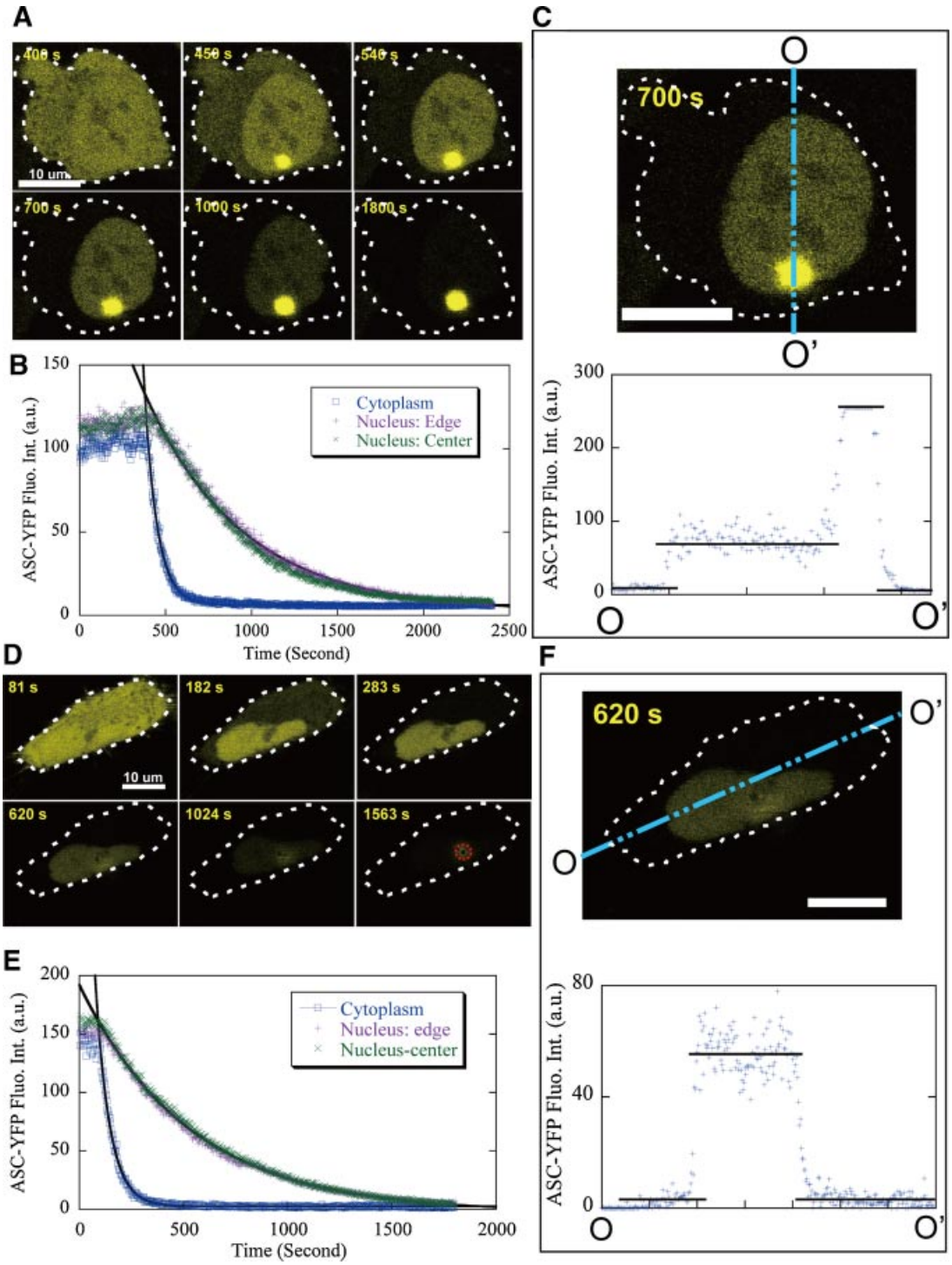

Fig. 5. Slower nuclear ASC depletion. Blue "□" data points are for cytoplasm, purple "+" for the nuclear edge, and green "×" for nuclear center locations inside the nucleus. All scale bars are 10 μm. A–C: Nuclear ASC depletion with the cytoplasmic speck on the same focal plane. A: Time-lapse image sequences. B: ASC fluorescence intensity at different nuclear locations and inside cytoplasm as a function of time ($\tau = 568 \pm 4$ sec for nuclear locations). C: A cross-section profile of ASC fluorescence intensity. D–F: The nuclear ASC depletion process with the speck on a different focal plane. D: Time-lapse image sequences, where the dashed circle indicates the speck location on a different focal plane. E: ASC fluorescence intensity at different nuclear locations and in the cytoplasm as a function of time ($\tau = 526 \pm 2$ sec for nuclear locations). F: A cross-section profile of ASC fluorescence intensity. [Color figure can be viewed in the online issue, which is available at www.interscience.wiley.com.]

observations. Thus, the simulations suggest that the binding of ASC to a speck is both efficient, with ~10% of collisions resulting in a binding event, and diffusion-limited, since even a modest decrease in the diffusion rate is predicted to cause inhomogeneities in soluble ASC distributions that are not observed.

Active transport along microtubules may be involved in some protein aggregation processes (Garcia-Mata et al., 1999). Since

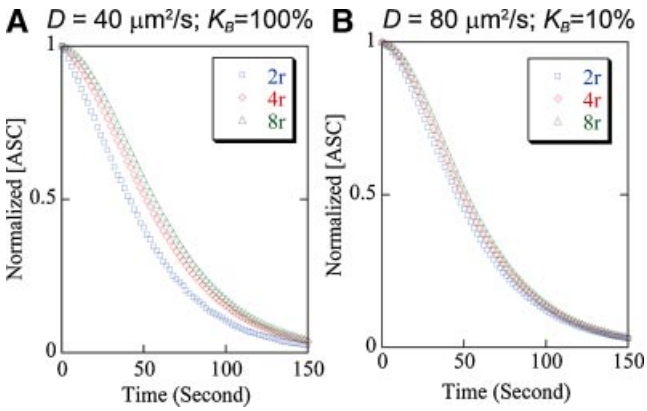

Fig. 6. Simulation of ASC aggregation during speck formation based on a free diffusion model. A: D = 40 μm²/sec and K_B = 100%. B: D = 80 μm²/sec and K_B = 10%. All other simulation parameters are taken from experimental measurements: 1.5 μm for mature speck radius (r) and 20 μm for cell radius. □: 2r distance from speck center, ◇: 4r, (: 8r. [Color figure can be viewed in the online issue, which is available at www.interscience.wiley.com.]

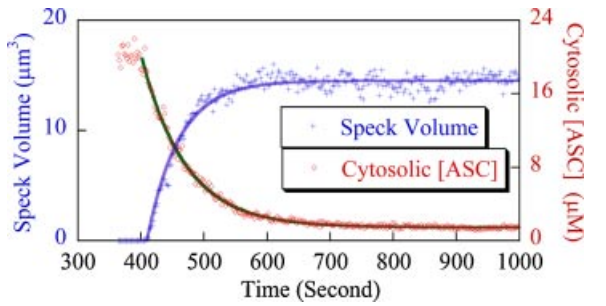

Fig. 7. ASC aggregation analysis during speck formation. The decreasing ASC concentration inside cytoplasm ("◇") and the corresponding increasing speck volume ("+"), where the solid lines are single exponential curve fits. Data correspond to Figure 5B. [Color figure can be viewed in the online issue, which is available at www.interscience.wiley.com.]

the majority of specks are localized near the microtubule-organizing center (MTOC), and since treatment of cells with the microtubule toxin nocodazole prevents ASC speck formation (Balci-Peynircioglu et al., 2008), motor proteins moving ASC molecules along microtubules seem to be an attractive possibility. Given the narrow range of parameters that can predict the kinetics of speck formation from diffusion, we considered whether active transport of ASC proteins might play a role during ASC speck formation (see Supporting Information for a detailed discussion). Active transport was modeled by assuming a hypothetical microtubule structure around the speck as a hub, on which motor proteins are assumed to transport ASC at a constant rate of speed. For all parameters, this model predicts that active transport results in an inhomogeneous ASC distribution during speck formation (Figs. S1 and S2) contrary to experimental observations. Therefore, we can reject this simplified active transport model and conclude that diffusion is most likely the dominant mechanism by which ASC moves to a speck, though we cannot exclude the possibility that some active transport is involved.

The energetics and kinetics of speck formation

Before ASC aggregation, the ASC concentration is estimated as 20 μM (see Supporting Information) and the equilibrium soluble ASC concentration in the cytosol ($[ASC]_{EQ}$) after ASC aggregation is complete can be estimated by the ratio of the cytosolic fluorescence intensity before and after ASC aggregation (i.e., $[ASC]_{EQ} \sim 0.007 \times 20 \sim 0.1$ μM). Therefore, the standard Gibbs free energy of the aggregation reaction can be calculated as $\Delta G^0 = -RT \ln(1/[ASC]_{EQ})$, or approximately −40 kJ/mol. Given the complexity of cytosolic biochemistry, our estimate of the cytosolic ASC concentration is potentially imprecise, but even large changes in ASC concentration do not greatly affect the free energy calculation. For example, even in an extreme case where the real ASC concentration is 10-fold higher (or lower) than estimated, the ΔG^0 would be approximately −35 (or −47) kJ/mol, respectively. These values approach the Gibbs free energy of ATP hydrolysis (ca. −50 kJ/mol) and almost double that of microtubule subunit polymerization (−15 to −25 kJ/mol) (VanBuren et al., 2002), supporting the idea that following the initial nucleation event, ASC aggregation is a highly favorable reaction. This also explains the dominance of aggregation during most of the speck formation process, such that disassociation events can be neglected, thus resulting in first-order reaction kinetics and the observed single exponential decay of the ASC concentration.

Figure 7 shows the change in soluble cytoplasmic ASC concentration over the course of speck formation. Additionally, the speck radius (r) is extracted from live-image sequences and the speck volume is calculated and plotted in Figure 7 as a function of time, assuming a spherical speck shape ($V = 4\pi r^3/3$). Clearly, the speck grows very fast initially, then slows down exponentially as the concentration of cytosolic ASC approaches 0, and finally asymptotically approaches the mature speck radius. The close correlation between cytosolic ASC depletion and increasing speck volume suggests that virtually all ASC proteins are recruited to form the speck.

ASC translocation across the nuclear envelope

The homogeneous location-independent ASC distribution inside/outside the nucleus during speck formation indicates that ASC diffusion occurs at a much faster rate than ASC transport across the nuclear envelope. The flux of ASC is outward when speck nucleation occurs in the cytoplasm, and nuclear ASC depletes about 10-fold slower than in the cytoplasm (Table 1). Speck formation within the nucleus is relatively rare: only a few events were observed during live cell imaging. In Figure 3D, imaging began after nuclear speck formation had initiated and only the later phases were captured. ASC was already depleted within the nucleus but was still dropping in the cytoplasm. In these cases, cytosolic ASC moves into the nucleus, where it aggregates onto the speck. ASC in the cytoplasm depletes at a rate comparable to that seen for nuclear depletion when a speck forms in the cytoplasm (Table 1). From the changing ASC concentration inside the nucleus, the peak rate that ASC moves across the nuclear envelope can be estimated at $\sim 10^4$ dimer/sec. Ribbeck and Gorlich (2001) estimated the free diffusion rate through a hypothetical

TABLE 1. Time constants of ASC depletion during speck formation (s)

Cytoplasmic ASC	Nuclear ASC	Note
46.4 ± 0.8	409 ± 10	Figure 3A
64 ± 2	529 ± 6	Figure 3B
64 ± 2	851 ± 487	Figure 3C
950 ± 16		Figure 3D (speck inside nucleus)
73.6 ± 0.4	568 ± 4	Figures 4E and 5E
67.6 ± 0.4	526 ± 2	Figures 4E and 5E

"plugless" nuclear pore complex (NPC) at roughly 400 molecules per second per micromole for concentration gradient of 100 kDa proteins. Considering ~2,800 nuclear pores per nucleus for HeLa cells (Ribbeck and Gorlich, 2001) and ~20 μM ASC peak concentration gradient, this would predict a peak rate for ASC dimers crossing the nuclear envelope of $\sim 2 \times 10^7$ molecules/sec. The 3-order magnitude difference of ASC translocation across the nuclear envelope between the plugless model and our experimental results suggests that ASC diffusion through the nuclear pores is substantially restricted. This restriction falls within the range of transport rates observed for other proteins in HeLa cells; for example, 4×10^6 molecules/sec for transportin (MW: 100 kDa) and $< 6 \times 10^3$ molecules/sec for bovine serum albumin (BSA) (MW: 68 kDa) at a 20 μM concentration gradient, based on the reported translocation rates of 65 NPC^{-1} sec^{-1} μM^{-1} for transportin and <0.1 NPC^{-1} sec^{-1} μM^{-1} for BSA (Ribbeck and Gorlich, 2001).

Discussion

The formation of protein aggregates is particularly important in the context of apoptosis and inflammation, where such aggregates can trigger proximity-induced activation of the effector molecules that mediate cell death and IL-1β processing. Since aggregated ASC can act as a cellular platform for both inflammatory processing and cell death, the study of its aggregation kinetics is of particular interest. Here, we track ASC aggregation during speck formation in non-myeloid cells and find highly nonlinear kinetics that lead to the rapid formation of a single speck within cells.

The ASC speck bears a striking morphological resemblance to a perinuclear protein aggregate called the aggresome (Garcia-Mata et al., 1999). Aggresomes, which, like specks are approximately 1.5 μm in diameter, form in response to the aggregation of misfolded proteins in the cell (Booth et al., 1997; Carrell and Gooptu, 1998). The inability of the cell to clear such insoluble protein aggregates is linked to pathogenesis of several degenerative disorders, including Alzheimer's disease, Parkinson's disease, amyloidosis, and the prion diseases (Horwich and Weissman, 1997; Ross and Poirier, 2004, 2005). Aggresome formation is a prelude to the initiation of cellular autophagy, a lysosome-mediated process by which the aggregated proteins can be cleared, and the cell can survive.

Time-lapse studies of aggresome formation indicate that the process of aggresome formation, which takes many hours (Garcia-Mata et al., 1999; Opazo et al., 2008), is orders of magnitude slower than that of speck aggregation, which takes minutes. In addition, the collapse of vimentin filaments in a cage-like structure around the aggresome is characteristic for this structure but is not seen upon speck formation. These findings indicate that specks and aggresomes are distinct structures.

Nevertheless, specks and aggresomes do share some features. Both form near the nucleus, co-localizing with the MTOC (Lee et al., 2002; Balci-Peynircioglu et al., 2008). Interference with the microtubule network of the cell by treatment with nocodozole inhibits speck formation (Balci-Peynircioglu et al., 2008) and also prevents aggresome formation (Johnston et al., 1998). In addition, the proteasome is recruited after the aggresome forms at the MTOC (Lee et al., 2002). We show here that ASC specks are only seen in cells with forming proteasomes and that the speck and the proteasome co-localize near the nucleus. These shared characteristics suggest that some functional features of speck and aggresome formation and/or some processes downstream from the generation of these complexes may be shared. For instance, since aggresomes trigger autophagy, it will be of interest to determine whether, in non-myeloid cells, formation of the ASC speck also promotes an autophagic reaction.

Like other types of protein aggregation (e.g., prion aggregation, amyloid formation), our results support a model of speck formation in which, under basal conditions, soluble ASC molecules have a low affinity for each other, leading to a very low probability of nucleating events. However, after nucleation occurs, the affinity of aggregated ASC for soluble ASC dramatically increases. Rapid, diffusion-limited recruitment of additional ASC quickly drives down the soluble ASC concentration. This aggregation step is remarkably efficient and its rapid rate makes the formation of a second speck in the same cell a highly unlikely event. Therefore, this mechanism ensures an abrupt, well-defined transition from the speck negative to the speck positive state. Since, in myeloid cells, speck formation is followed quickly by caspase-1-dependent death (pyroptosis), such an abrupt onset and well-defined end state could serve to ensure an all or none commitment to inflammatory cell death. However, here we find that speck formation in non-myeloid cells also follows quickly after nucleation, despite the fact that death after speck formation may be delayed by 72 h or more in these cells (Schaner et al., 2001). This delay suggests that the speck platform has some as yet unrecognized function in non-myeloid cells.

It is possible to predict some additional characteristics of speck formation from analysis of their aggregation kinetics. Based on collision theory in solution (Cox, 1994), the collision rate of solute molecules can be estimated given their concentration, molecular size, and diffusion coefficient (see Supporting Information). From the estimated 20 μM ASC concentration, the collision rate of two free ASC dimers prior to speck formation is calculated to be approximately 6×10^{11} sec^{-1} per cell. Even if the concentration is an order of magnitude less, the collision rate still remains very high, though decreased by 2 orders of magnitude to 6×10^9 sec^{-1} per cell because of the second-order kinetics. Yet specks form in less than 2% of cells containing ASC-YFP during the 30 min observation window, yielding the speck nucleation rate of less than 10^{-5} sec^{-1} per cell, giving a miniscule probability $\sim 10^{-16}$ of a collision resulting in speck nucleation. However, after nucleation, the probability that ASC will adhere upon colliding with the nascent speck rises drastically by 15 orders of magnitude to 10%. Consequently, ASC is rapidly depleted so that the probability of a second speck forming is extremely low—indeed a second speck was never observed during the confocal microscopy studies.

The combination of a high ASC collision rate, coupled with a low probability of speck nucleation, suggests that the kinetics of speck nucleation are a much higher than a second-order process. A crude estimate of the order of the nucleation process can be estimated by a dimensional argument (see Supporting Information). Based on the observations that speck nucleation rate is less than 10^{-5} sec^{-1} per cell and the total calculated collision number of multiple-ASC collision rate ($\sim 10^{-4}$ sec^{-1} per cell for 15-ASC collision and $\sim 10^{-6}$ sec^{-1} per cell for 16-ASC collision), a lower bound of 15th-order speck nucleation process is estimated. Although this is subject to great uncertainty given that we cannot estimate the probability that such a collision will produce a nucleus, we can less exactly conclude that speck formation is "high order."

It is also remarkable that once the nucleation event occurs, the process of ASC aggregation transforms from an extremely low probability event to an extremely high probability and high affinity event. In this respect, the process of ASC aggregation is analogous to protein aggregation events in amyloid or prion diseases, where fibril formation happens rapidly once a rare seed formation occurs (Weissmann, 2004). The kinetics of speck formation, however, far outpace that of any of the misfolded protein aggregation pathways, including aggresome formation (Garcia-Mata et al., 1999; Opazo et al., 2008). This kinetics makes speck formation one of the fastest known

protein aggregation events. Further study of the protein determinants of this process will be an important future goal for biochemists and cell biologists.

Acknowledgments

We thank Dr. M.J. Solomon and his group members at the Department of Chemical Engineering, and Dr. Y.M. Yamashita at Life Science Institute, The University of Michigan for the laser scanning confocal microscope usage and support. This work was supported by NIH grants to A.J.H. (R01-GM072006) and to D.L.G. (R01-AI53262).

Literature Cited

Akahira J, Sugihashi Y, Ito K, Niikura H, Okamura K, Yaegashi N. 2004. Promoter methylation status and expression of TMS1 gene in human epithelial ovarian cancer. Cancer Sci 95:40–43.

Alumkal JJ, Zhang Z, Humphreys EB, Bennett C, Mangold LA, Carducci MA, Partin AW, Garrett-Mayer E, Demarzo AM, Herman JG. 2008. Effect of DNA methylation on identification of aggressive prostate cancer. Urology 72:1234–1239.

Balci-Peynircioglu B, Waite AL, Schaner P, Taskiran ZE, Richards N, Orhan D, Gucer S, Ozen S, Gumucio D, Yilmaz E. 2008. Expression of ASC in renal tissues of familial Mediterranean fever patients with amyloidosis: Postulating a role for ASC in AA type amyloid deposition. Exp Biol Med (Maywood) 233:1324–1333.

Booth DR, Sunde M, Bellotti V, Robinson CV, Hutchinson WL, Fraser PE, Hawkins PN, Dobson CM, Radford SE, Blake CC, Pepys MB. 1997. Instability, unfolding and aggregation of human lysozyme variants underlying amyloid fibrillogenesis. Nature 385:787–793.

Carrell RW, Gooptu B. 1998. Conformational changes and disease—Serpins, prions and Alzheimer's. Curr Opin Struct Biol 8:799–809.

Conway KE, McConnell BB, Bowring CE, Donald CD, Warren ST, Vertino PM. 2000. TMS1, a novel proapoptotic caspase recruitment domain protein, is a target of methylation-induced gene silencing in human breast cancers. Cancer Res 60:6236–6242.

Cox BG. 1994. Modern liquid phase kinetics. Oxford; New York: Oxford University Press.

Fernandes-Alnemri T, Alnemri ES. 2008. Chapter Thirteen: Assembly, purification, and assay of the activity of the ASC pyroptosome. Methods Enzymol 442:251–270.

Fernandes-Alnemri T, Wu J, Yu JW, Datta P, Miller B, Jankowski W, Rosenberg S, Zhang J, Alnemri ES. 2007. The pyroptosome: A supramolecular assembly of ASC dimers mediating inflammatory cell death via caspase-1 activation. Cell Death Differ 14:1590–1604.

Fink SL, Cookson BT. 2006. Caspase-1-dependent pore formation during pyroptosis leads to osmotic lysis of infected host macrophages. Cell Microbiol 8:1812–1825.

Fushimi K, Verkman AS. 1991. Low viscosity in the aqueous domain of cell cytoplasm measured by picosecond polarization microfluorimetry. J Cell Biol 112:719–725.

Garcia-Mata R, Bebok Z, Sorscher EJ, Sztul ES. 1999. Characterization and dynamics of aggresome formation by a cytosolic GFP-chimera. J Cell Biol 146:1239–1254.

Guan X, Sagara J, Yokoyama T, Koganehira Y, Oguchi M, Saida T, Taniguchi S. 2003. ASC/TMS1, a caspase-1 activating adaptor, is downregulated by aberrant methylation in human melanoma. Int J Cancer 107:202–208.

Gumucio DL, Diaz A, Schaner P, Richards N, Babcock C, Schaller M, Cesena T. 2002. Fire and ICE: The role of pyrin domain-containing proteins in inflammation and apoptosis. Clin Exp Rheumatol 20:S45–S53.

Horwich AL, Weissman JS. 1997. Deadly conformations—Protein misfolding in prion disease. Cell 89:499–510.

Johnston JA, Ward CL, Kopito RR. 1998. Aggresomes: A cellular response to misfolded proteins. J Cell Biol 143:1883–1898.

Lee HJ, Shin SY, Choi C, Lee YH, Lee SJ. 2002. Formation and removal of alpha-synuclein aggregates in cells exposed to mitochondrial inhibitors. J Biol Chem 277:5411–5417.

Luby-Phelps K, Mujumdar S, Mujumdar RB, Ernst LA, Galbraith W, Waggoner AS. 1993. A novel fluorescence ratiometric method confirms the low solvent viscosity of the cytoplasm. Biophys J 65:236–242.

Mariathasan S, Weiss DS, Newton K, McBride J, O'Rourke K, Roose-Girma M, Lee WP, Weinrauch Y, Monack DM, Dixit VM. 2006. Cryopyrin activates the inflammasome in response to toxins and ATP. Nature 440:228–232.

Martinon F. 2008. Detection of immune danger signals by NALP3. J Leukoc Biol 83:507–511.

Martinon F, Petrilli V, Mayor A, Tardivel A, Tschopp J. 2006. Gout-associated uric acid crystals activate the NALP3 inflammasome. Nature 440:237–241.

Masumoto J, Taniguchi S, Ayukawa K, Sarvotham H, Kishino T, Niikawa N, Hidaka E, Katsuyama T, Higuchi T, Sagara J. 1999. ASC, a novel 22-kDa protein, aggregates during apoptosis of human promyelocytic leukemia HL-60 cells. J Biol Chem 274:33835–33838.

McConnell BB, Vertino PM. 2000. Activation of a caspase-9-mediated apoptotic pathway by subcellular redistribution of the novel caspase recruitment domain protein TMS1. Cancer Res 60:6243–6247.

Moriai R, Tsuji N, Kobayashi D, Yagihashi A, Namiki Y, Takahashi H, Watanabe N. 2002. A proapoptotic caspase recruitment domain protein gene, TMS1, is hypermethylated in human breast and gastric cancers. Anticancer Res 22:4163–4168.

Opazo F, Krenz A, Heermann S, Schulz JB, Falkenburger BH. 2008. Accumulation and clearance of alpha-synuclein aggregates demonstrated by time-lapse imaging. J Neurochem 106:529–540.

Petrilli V, Dostert C, Muruve DA, Tschopp J. 2007. The inflammasome: A danger sensing complex triggering innate immunity. Curr Opin Immunol 19:615–622.

Ribbeck K, Gorlich D. 2001. Kinetic analysis of translocation through nuclear pore complexes. EMBO J 20:1320–1330.

Richards N, Schaner P, Diaz A, Stuckey J, Shelden E, Wadhwa A, Gumucio DL. 2001. Interaction between pyrin and the apoptotic speck protein (ASC) modulates ASC-induced apoptosis. J Biol Chem 276:39320–39329.

Ross CA, Poirier MA. 2004. Protein aggregation and neurodegenerative disease. Nat Med 10:S10–S17.

Ross CA, Poirier MA. 2005. Opinion: What is the role of protein aggregation in neurodegeneration? Nat Rev Mol Cell Biol 6:891–898.

Schaner P, Richards N, Wadhwa A, Aksentijevich I, Kastner D, Tucker P, Gumucio D. 2001. Episodic evolution of pyrin in primates: Human mutations recapitulate ancestral amino acid states. Nat Genet 27:318–321.

Swanson MS, Molofsky AB. 2005. Autophagy and inflammatory cell death, partners of innate immunity. Autophagy 1:174–176.

Terasawa K, Sagae S, Toyota M, Tsukada K, Ogi K, Satoh A, Mita H, Imai K, Tokino T, Kudo R. 2004. Epigenetic inactivation of TMS1/ASC in ovarian cancer. Clin Cancer Res 10:2000–2006.

Tyn M, Gusek T. 1990. Prediction of diffusion-coefficients of proteins. Biotechnol Bioeng 35:327–338.

VanBuren V, Odde DJ, Cassimeris L. 2002. Estimates of lateral and longitudinal bond energies within the microtubule lattice. Proc Natl Acad Sci USA 99:6035–6040.

Virmani A, Rathi A, Sugio K, Sathyanarayana UG, Toyooka S, Kischel FC, Tonk V, Padar A, Takahashi T, Roth JA, Euhus DM, Minna JD, Gazdar AF. 2003. Aberrant methylation of TMS1 in small cell, non small cell lung cancer and breast cancer. Int J Cancer 106:198–204.

Weissmann C. 2004. The state of the prion. Nat Rev Microbiol 2:861–871.

Yokoyama T, Sagara J, Guan X, Masumoto J, Takeoka M, Komiyama Y, Miyata K, Higuchi K, Taniguchi S. 2003. Methylation of ASC/TMS1, a proapoptotic gene responsible for activating procaspase-1, in human colorectal cancer. Cancer Lett 202:101–108.